

Escape dynamics of a self-propelled nanorod from circular confinements with narrow openings

Praveen Kumar and Rajarshi Chakrabarti*

Department of Chemistry, Indian Institute of Technology Bombay, Mumbai 400076, India

We perform computer simulations to explore the escape dynamics of a self-propelled (active) nanorod from circular confinements with narrow opening(s). Our results clearly demonstrate how the persistent and directed motion of the nanorod helps it to escape. Such escape events are absent if the nanorod is passive. To quantify the escape dynamics, we compute the radial probability density function (RPDF) and mean first escape time (MFET) and show how the activity is responsible for the bimodality of RPDF, which is clearly absent if the nanorod is passive. The broadening of displacement distributions with activity has also been observed. The computed mean first escape time decreases with activity. In contrast, the fluctuations of the first escape times vary in a non-monotonic way. This results high values of the coefficient of variation and indicates the presence of multiple timescales in first escape time distributions and multimodality in uniformity index distributions. We hope our study will help in differentiating activity-driven escape dynamics from purely thermal passive diffusion in confinement.

I. INTRODUCTION

The “narrow escape problem” is an omnipresent phenomenon in areas like biophysics, polymer physics, cellular biology, *etc.* [1–5]. As the name suggests, this refers to a range of phenomena where a molecule or a nano or micron-sized object escapes from confinements through narrow opening(s). Examples from biology include ion transport through ion channels made of proteins, proteins trafficking through nuclear pore complex (NPC) or passing through mucus membrane, and bacteria motion through disordered media where it moves between the confined domains connected by narrow channels [4, 6–10]. In particular, the movement of proteins between two chambers *via* a narrow opening is an example of a narrow escape problem. In polymer physics, translocation is a type of phenomenon that involves the transport of macromolecules through a narrow opening and is, therefore, closely related to the narrow escape problem [11–13]. One way to quantify the narrow escape problem is to compute the mean first-passage time, which is the average time to exit through the opening [4, 14–16]. In recent years, narrow escape problems have received increasing attention from researchers due to their relevance and potential applications in diverse fields, such as cellular biophysics, site-specific delivery of drugs, and nonviral gene delivery [1–3, 17, 18].

The escape dynamics of passive Brownian walkers from different types of confined geometries have been extensively studied, both experimentally and theoretically [3, 11, 12, 15, 16, 19–26]. Therein, the escape dynamics of the passive particles has been analyzed by varying the control parameters, such as the shape and volume of confined geometries, the size of the pore and the randomly moving particle, and the number of openings

(small pores) [15, 16, 21, 22, 24, 27]. Thus, the escape dynamics of passive Brownian particles from confined regions represent a complex interplay among these factors, the properties of the surrounding environments, and the nature of the escaping particles [2, 3, 6, 7, 23, 28–31].

The diffusion of self-propelled objects in complex environments is a fascinating and promising area of research that still offers ample opportunities for further exploration and investigation [32–41]. It becomes even more interesting when self-propelled objects navigate through confined geometries with narrow openings [42, 43]. Here, the term self-propelled objects refers to biological or artificial agents that consume energy from the environment or utilize their internal chemical energy to get directed motion in a complex environment [44, 45]. Examples include biological entities such as bacteria [46, 47], spermatozoa [48], insects, and animals [49, 50] and synthetic systems such as self-propelled Janus rods, discs, light-induced active particles, and chemically driven systems [45, 51–57]. Furthermore, because of the additional energy sources, these objects are typical non-equilibrium systems with peculiar transport and collective properties [45, 46, 58–60].

In recent years, some theoretical and experimental studies have been reported on the quantification of the mean first passage time of the self-propelled particles in confined geometries, such as a Petri dish, a pie-wedge shape, and various shaped confinements with narrow openings [43, 61–67]. A very recent experimental study reported that the mean first passage times of an active particle rise monotonically as a function of the area fraction of the surrounded passive discs (crowders), while their fluctuations exhibit non-monotonic behavior [61]. Debnath *et al.* numerically investigated the mean exit time of an active particle from circular confinement with single or multiple exit windows, and they observed that overdamped active particles spread on the surface

* rajarshi@chem.iitb.ac.in

of the confinement at extensive self-propulsion lengths and rotational dynamics governs the escape process [43]. A recent numerical study investigated the effect of motility parameters on the narrow escape time of active particles from circular domains [66]. This study compared two paradigmatic models of active motions, namely, run-and-tumble and active Brownian. It has been found that run-and-tumble particles are less efficient in escaping from the chamber compared to active Brownian particles at equal persistence times in the active limit. The escape dynamics from a circular disk for interacting active particles has further been extended using a minimal two-dimensional Vicsek model [65]. The results of this study revealed that the survival probability for noninteracting particles is exponential, whereas the interacting particles have an exciting crossover of survival probability from initial exponential to subexponential late-time decay. In a very recent study, it has been shown how worms escape from one confined domain to another through a narrow channel [67]. Mostly, previous attempts focused on the confinement shape and relative size of the active particle to the small pore and the effect of crowding to study the escape dynamics. However, much less is explored on the effect of the shape of particles on their dynamics inside bounded domains with a single and multiple narrow opening(s). Anisotropy in shape leads to more complicated dynamical behaviors. Additionally, the presence of multiple targets in the form of small openings complicates the escape dynamics from the confinement. The role of confinement on the dynamics of active particles is unquestionably critical in realistic systems, particularly for biological matter and biotechnology. Even though there has been some progress to date, a lot of fundamental questions still need to be resolved. For instance, how the self-propulsion and the number of openings located on the boundary affect the escape dynamics of the nanorod from the circular domain. The fields of “active transport” and “narrow escape” are currently of great interest, and this work serves as an example that integrates both of these research topics.

In this paper, we study the narrow escape dynamics of a self-propelled rigid nanorod confined to an impenetrable circular domains with single and multiple narrow openings (small open windows) through which the nanorod may escape [Fig. 2(A-C)]. We perform Brownian dynamics simulations to unveil the escape dynamics of a self-propelled nanorod through the narrow opening(s). For this purpose, we analyze the dynamics and statistics of the first escape times for the nanorod. We compute the radial probability density function by following the centre of mass (COM) position r_c of the rigid nanorod. We found that a passive nanorod shows restricted movement inside the circular confinement, whereas the self-propelled nanorod moves faster, reaches the boundary, and escapes through the narrow opening(s) present at the boundary. This escape is assisted by the persistent

and directed motion of the nanorod. Our analyses of the self-part of the van-Hove correlation function of the nanorod show that the correlations become flat at higher displacement and broader with shoulder peaks by increasing the self-propulsion. In addition, the mean first escape (exit) times of the self-propelled nanorod monotonically decrease by increasing the activity and the number of narrow openings on the boundary of the confinement. At the same time, their fluctuations (coefficient of variation CV) show non-monotonic behavior. To understand the fluctuations in trajectories (first escape times), we look at the full distribution $F(\tau_{es})$ and uniformity index distribution $P(\omega)$ of random first escape times of the active nanorod. We believe that our investigations contribute to understanding the escape dynamics of a biomimetic object of elongated shape, a nanorod in this case, from confined geometries with small open windows.

This paper is organized as follows. In Section II, we explain the model system investigated in the present work. First, we describe the method for computationally constructing the self-driven rigid nanorod, which diffuses inside the circular rigid confinement and escapes through a small window. Thereafter, we describe the simulation protocol employed in our simulation study. Results and discussion are presented in Section III. Finally, we conclude the paper in Section IV.

II. MODEL AND SIMULATION DETAILS

We model the microswimmer as a self-driven rigid nanorod which is composed of five beads, each with an identical diameter σ and mass m , where σ has the dimension of length. The beads of the nanorod are connected by harmonic potential, denoted by V_{harmonic} , and expressed as follows:

$$V_{\text{harmonic}}(r_{ij}) = k_{\text{H}} \frac{(r_{ij} - r_0)^2}{2} \quad (1)$$

here k_{H} is the spring constant and r_0 represents the equilibrium distance between two neighboring beads of the nanorod, which is constant throughout the simulations. Thus, the nanorod has a fixed length of 5σ . We ensure that the nanorod always moves and rotates as a single rigid body. Next, circular confinement with different numbers of narrow openings is modeled as rigid circular confinement with a radius of 16σ , and the boundary (circumference) of the confinement is made of circular beads of diameter σ [see Fig. 1 for the confinement with a single narrow opening]. Each of the narrow openings is created by removing a pair of particles from the boundary of the confinement so that the size of each narrow opening (small window) is fixed ($\delta l \sim 2\sigma$), which is much smaller than the size of circular

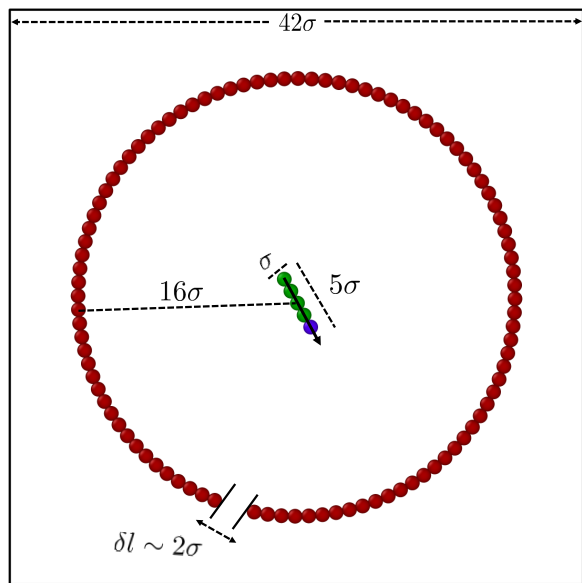


Fig. 1. The snapshot of a self-driven nanorod of length 5σ inside a circular confinement with a single narrow opening. The size of the narrow opening is around $\delta l = 2\sigma$, which is created by removing the pair of particles from the circumference of the ring confinement. The black arrow indicates the direction of self-propulsion. Ovito package is used to generate this snapshot [70].

rigid confinement and also much smaller than the length of the nanorod. This ensures that the nanorod can only escape through these holes/openings head-on. The circular domain is enclosed in a two-dimensional square box with edge length 42σ . The center of the ring confinement is fixed at the coordinates $(0,0)$ of the box during the simulations. The rigid nanorod with random orientation is carefully placed at the center of the circular rigid confinement with the narrow opening(s) through which it can exit or enter. To accurately capture the entire process of escape and reentry of a self-driven rigid nanorod through a narrow opening, we have set the length of the simulation box to be ten units larger than the size of the circular confinement. In this work, we systematically investigated three cases by changing the number of small openings in the system, specifically by examining cases with a single opening, three openings, and five openings. These openings, referred to as small pores or windows, are intentionally positioned in a well-separated manner. Here, we aim to gain insights into how the number of openings influences the escape dynamics of the nanorod from the circular confinement [27, 68]. Confinements or domains with multiple small openings can be seen as a scenario where search processes occur for multiple targets. Mostly, previous models related to narrow escape problems (first passage time problems) focused on a single target (exit) in a given search domain [14, 15, 24, 66, 69].

The non-bonded pairwise interactions between all the particles of the confinement and the nanorod are set as purely repulsive and modeled by Weeks–Chandler–Andersen (WCA) potential [71]:

$$V_{\text{WCA}}(r_{ij}) = \begin{cases} 4\epsilon_{ij} \left[\left(\frac{\sigma_{ij}}{r_{ij}} \right)^{12} - \left(\frac{\sigma_{ij}}{r_{ij}} \right)^6 \right] + \epsilon_{ij}, & \text{if } r_{ij} < r_{\text{cut}} \\ = 0, & \text{otherwise} \end{cases} \quad (2)$$

where $r_{\text{cut}} = 2^{1/6}\sigma_{ij}$, $\sigma_{ij} = \frac{\sigma_i + \sigma_j}{2}$, with $\sigma_{i(j)}$ being the diameter of the interacting pairs. $\epsilon_{ij} = 1$ and r_{ij} are the strength of the steric repulsion and the distance between the interacting particles, respectively.

The following Langevin equation is implemented to describe the dynamics of each particle with mass m and position $\mathbf{r}_i(t)$ at time t ,

$$m \frac{d^2 \mathbf{r}_i(t)}{dt^2} = -\gamma \frac{d\mathbf{r}_i}{dt} - \sum_j \nabla V(\mathbf{r}_i - \mathbf{r}_j) + \mathbf{f}_i(t) + \mathbf{F}_a \hat{\mathbf{n}} \quad (3)$$

where γ is the friction coefficient, which is very high (5.3×10^4) in our simulations so that the underlying dynamics is effectively overdamped. $V(r) = V_{\text{harmonic}} + V_{\text{WCA}}$ is the resultant interaction potential of the system [Eq. 1 and Eq. 2]. Thermal fluctuations are captured by the Gaussian random force $\mathbf{f}_i(t)$, satisfying the fluctuation-dissipation theorem.

$$\langle f(t) \rangle = 0, \quad \langle f_\alpha(t') f_\beta(t'') \rangle = 4k_B T \gamma \delta_{\alpha\beta} \delta(t' - t'') \quad (4)$$

where k_B is the Boltzmann constant, T is the temperature, and δ represents the Dirac delta function. α and β are the Cartesian components. The activity is introduced as a propulsive force $\mathbf{F}_a \hat{\mathbf{n}}$, where F_a represents the magnitude of the constant self-propulsion with orientation specified by the unit vector $\hat{\mathbf{n}}$ along the body axis of the nanorod. The inclusion of active force breaks the fluctuation-dissipation theorem. In the present study, the Lennard-Jones parameters σ , ϵ , and mass m are the fundamental units of length, energy, and mass, respectively. All other physical quantities are therefore reduced accordingly and expressed in terms of the fundamental units σ , ϵ , and mass m , and presented in dimensionless forms. The energy and time units have been designated as $k_B T$ and $\sqrt{\frac{m\sigma^2}{k_B T}}$, respectively. To measure the strength of active force (self-propulsion), we express it in terms of a dimensionless quantity Péclet number Pe , defined as $\frac{F_a \sigma}{k_B T}$. Therefore, $\text{Pe} = 0$ corresponds to the passive nanorod.

All simulations are performed in a square box with periodic boundary conditions in all directions. We use Langevin thermostat by employing the LAMMPS package [72], and the equation of motion [Eq. 3] is integrated using the velocity Verlet algorithm in each

time step. All the production simulations are carried out for 5×10^8 steps, and the simulation integration time step is set to be 5×10^{-4} . We record the positions of the particles for every 100th step.

We have carried out 150 independent simulations for a given value of Pe and the number of openings, n_o . The Pe values considered here are 0, 2, 5, 10, 20, and 40, where Pe = 0 stands for the passive case. We consider three values of n_o , *viz.* $n_o = 1$ (a single opening), $n_o = 3$ (three openings), and $n_o = 5$ (five openings). For each case, every simulation starts therefore placing the nanorod at the centre of the confinement, and they run independently.

III. RESULTS AND DISCUSSION

A. Dynamics and interaction of the nanorod with the boundary of the confinement

In order to understand the escape dynamics of a self-driven nanorod from the circular confinement through narrow opening(s), we first compute the radial probability density function (RPDF) $P(r_c)$ of finding the nanorod at different active forces (Pe) for all three cases ($n_o = 1, 3, 5$), as shown in Fig.2(A-C). Here, r_c is the centre of mass (COM) position of the nanorod. In this study, the radial probability density functions are normalized so the total area under each RPDF curve equals unity. From Fig. 2(D-F), we notice that the passive (Pe = 0) nanorod has almost equal probability all over the place inside ($r_c < 16\sigma$) the circular confinement but drops at the boundary. This indicates the passive nanorod diffuses smoothly inside the confinement with no particular preference to the boundary of the circular confinement [see ESI videos, Movies S1-S3 for $n_o = 1, 3$, and 5, respectively]. As mentioned, $P(r_c)$ drops quite sharply close to the boundary, which accounts for the repulsive interaction between the nanorod and the boundary particles. This observation ensures that the passive nanorod since has no attractive interaction with the boundary, it spends most of its time away from the boundary and therefore never escapes through the opening(s) present at the boundary. At least, we do not capture any escape events for the passive nanorod in our simulations. In all the cases with Pe > 0, RPDFs are bimodal and these bimodal distributions have two peaks with maxima, one inside and the other outside the circular confinement [Fig. 2(D-F)]. This indicates that the active nanorod escapes through the narrow opening(s). The peaks inside the confinement appear around $r_c \approx 14\sigma$ (the boundary is at 16σ), indicating the fact that the active nanorod has spent most of its time close to the boundary. In the case of an active nanorod, there are events where the active nanorod goes to the boundary and persistently pushes the boundary before

rotating and moving along the boundary. This can also be seen clearly in ESI videos Movies S7 and S15. This is a characteristic of active Brownian particle (ABP), a result of its persistent motion. Escape events of active nanorods can also be clearly seen from ESI videos, namely, Movies S4, S5, and S6 for all three cases. This requires a proper alignment of the nanorod in proximity to the boundary. To support this understanding, we have taken some snapshots from the simulation of the nanorod successfully escaping through various narrow openings present on the confinement's boundary. These snapshots depict different orientations of the nanorod with respect to the openings during the escape process [Fig. S2, ESI]. Conversely, we have also taken snapshots where the nanorod is in close proximity to the hole but still unable to escape due to its improper orientation, as it appears to be nearly parallel to the wall [Fig. S3, ESI]. On the other hand, the second peak at $r_c \approx 19\sigma$ represents the probability of finding the active nanorod outside the confinement when it is sticking to the impenetrable boundary. But this sticking is due to its persistent motion when aligned roughly perpendicular to the boundary wall from outside. This happens without any sticky LJ (Lennard-Jones) interaction of the nanorod with the boundary. This mode of approach actually helps the nanorod to re-enter through the opening(s). We manifest that the nanorod prefers to stay outside, close to the boundary of the confinement, until it gets a chance to re-enter the circular domain. In addition, a second sharp peak outside the confinement starts appearing at $r_c \approx 17\sigma$ with increasing Pe. It would be another possible approach for the nanorod to the boundary wall, where it is sliding against the wall rather than sticking to it. Both of these are captured in $P(r_c)$ peaks outside the confinement.

A careful observation shows that these apparently bimodal distributions have finer structures. The broad peak inside the confinement, on increasing Pe, becomes sharper and shifts close to the boundary. The same happens with the peak outside the confinement, it sharpens and shifts close to the boundary. This may be seen in the ESI videos, namely Movies S7, S8, and S9, at a higher Pe = 20 for all three cases. We also note that the probability of finding the active nanorod decreases inside while increasing outside the confinement at a higher activity (Pe = 40), as the heights of the peaks reflect in $P(r_c)$ [Fig. 2(D-F)]. Similar behavior is observed for all three cases, namely single, three, and five narrow opening(s). Furthermore, the radial probability distributions are supported by the corresponding plots of the COM trajectory of the nanorod, as shown in Fig. 2(G-I). From the trajectories, we can see clearly that the nanorod has uniform spreading inside the confinement in the passive case, while the active nanorod has circular spreading along the boundary.

In Fig. 3(A-C), we compare the radial probability dis-

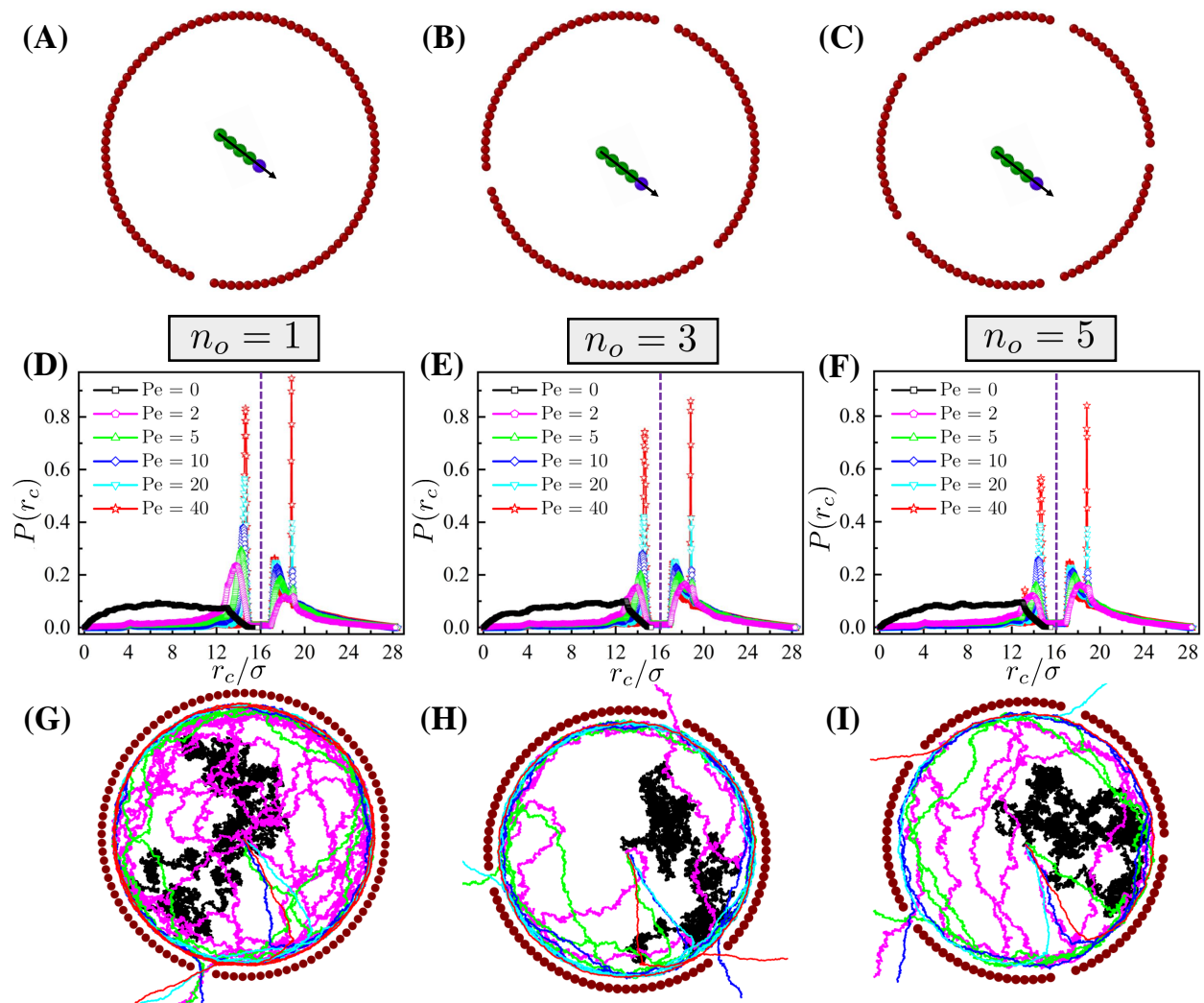


Fig. 2. The snapshots of a self-driven nanorod inside a circular confinements with (A) single, (B) three, and (C) five narrow opening(s) through which the nanorod escapes or enters the confinement. The self-propulsion is directed from green to blue beads, and the arrow represents it in (A), (B), and (C). The radial probability density distributions ($P(r_c)$) of the nanorod for the confinement with single, three, and five opening(s) at different activities (Pe) are shown in (D), (E), and (F), respectively. The corresponding COM trajectories of the nanorod in (D), (E), and (F) are shown in (G), (H), and (I), respectively, for different Pe . The dashed purple vertical lines at $r_c = 16\sigma$ in (D), (E), and (F) represent the boundary of the domain, where $r_c < 16\sigma$ and $r_c > 16\sigma$ are the inside and outside of the confinement, respectively.

tributions by changing the number of narrow openings while keeping Pe constant. By increasing the number of narrow openings, the number of events having escape and re-entrance increases, leading to a decrease in the probability of finding the active nanorod near the boundary of the confinement. The presence of multiple openings in confinement increases the accessibility and options for the active nanorod to find an escape route. This results in an increased probability of successful escape and re-entry for the nanorod, enhancing its ability to overcome confinement. This can also be clearly seen in ESI videos, namely Movies S5, S6, S8, and S9. Self-propulsion, as well as the number of narrow openings, play a crucial role in assisting the escape of

nanorods from confinement. The presence of extended long tails away from the circular wall in the profile of $P(r_c)$ provide insights into the position probability distribution of the active nanorod both inside and outside of the confinement [Fig. 2(D-F) and Fig. 3]. This behavior leads to a low probability of finding the nanorod away from the circular wall. Additionally, we explored a scenario without any narrow openings on the confinement's boundary, and remarkably, the extended tails outside the circular wall in the profile of $P(r_c)$ disappear [Fig. S4, ESI] [36]. These long tails outside the wall are a consequence of the narrow opening(s) present on the confinement's boundary.

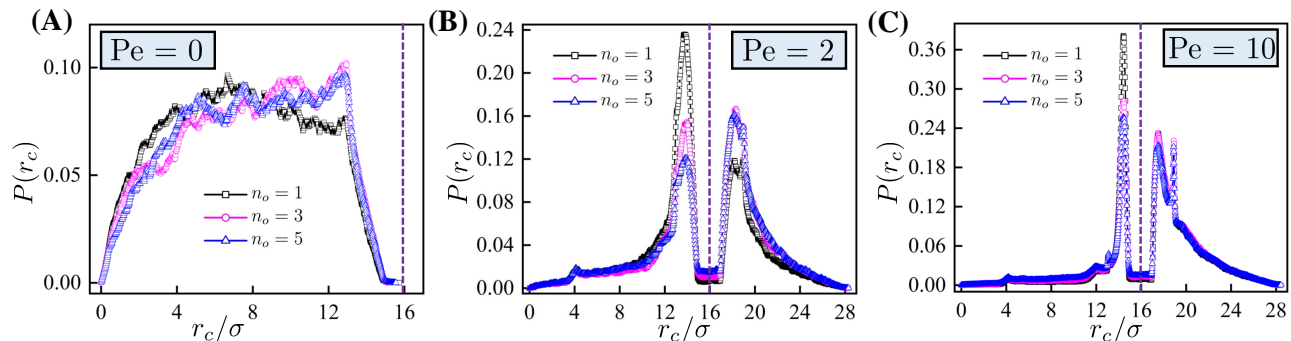


Fig. 3. $P(r_c)$ of the self-propelled nanorod at (A) $Pe = 0$, (B) $Pe = 2$, and (C) $Pe = 10$ for confinements with single, three, and five opening(s). The dashed purple vertical lines at $r_c = 16\sigma$ represent the boundary of the circular domain.

In addition, to have an even deeper understanding of the nanorod motion, we analyze the self part of the van-Hove correlation function (the displacement probability distribution function) defined as $P(\Delta x_c; \tau) \equiv \langle \delta(\Delta x - (x_c(t + \tau) - x_c(t))) \rangle$ of the nanorod in one dimension, where $x_c(t + \tau)$ and $x_c(t)$ are the COM positions of the nanorod along x -direction at time $(t + \tau)$ and t , respectively. We compute the van-Hove self-correlation functions for a given time interval τ and study the effect of self-propulsion on $P(\Delta x_c)$ by varying Pe [Fig. 4]. The distribution curves for a passive ($Pe = 0$) and weakly active ($Pe = 2$) nanorod overlap, but the nanorod with high self-propelled velocities tends to have even broader and flatter distributions. This is consistent with the larger displacement of the active nanorod, both inside and outside the confinement [Fig. 4(A-C)]. More interestingly, there exist shoulder peaks in $P(\Delta x_c; \tau)$ at higher values of Pe . We also observed the shoulder peaks for moderate activities (say, $Pe = 5, 10$), but at larger τ [Fig. 4C]. This is a consequence of the impenetrable circular boundary, where the active nanorod stays for a longer time due to its directed motion toward the boundary. Typically, the particle with high self-propulsion tends to move towards the boundary of the confinement and escapes if it gets a chance [32, 36, 73]. Similar distributions of displacements are observed earlier in an experimental study of an active particle confined to a glass Petri dish [61]. Furthermore, the flattening of the van-Hove distribution indicates that at higher self-propulsion, the nanorod moves freely inside and outside the confinement. In other words, shorter and larger displacements Δx_c become equally probable. This behavior indicates that the nanorod has increased mobility and escape capability at higher Pe . Moreover, we also depict trial fittings of these van-Hove distributions with a Gaussian distribution, $P_g(\Delta x_c; \tau) = \frac{1}{\sqrt{2\pi\langle \Delta x_c^2 \rangle}} \exp\left(-\frac{\Delta x_c^2}{2\langle \Delta x_c^2 \rangle}\right)$. Therefore, any deviation of the van-Hove distributions from the Gaussian curves indicates non-Gaussianity [Fig. S5, ESI]. We found that the distributions are Gaussian for a given τ in the case of passive nanorod, whereas $P(\Delta x_c)$ starts deviating from the Gaussianity with increasing Pe owing to the self-driven motion of the nanorod. The de-

viation from Gaussianity becomes more pronounced at larger values of τ and Pe . These findings contribute to a better understanding of the effect of self-propulsion on nanorods in confined domains and their subsequent escape.

B. Analyses of escape time

Utilizing our existing knowledge of dynamics and the interaction of the nanorod with the boundary, we next discuss the results for the statistics of first escape times and specifically highlight the non-monotonic variation of first escape times by varying the magnitude of the active force and the number of narrow openings. We compute the mean first escape time (MFET), defined as the time taken by the particle to reach the boundary of the domain and escape through a narrow opening, as defined and used in the literature [14, 25, 27, 31, 61, 67, 69, 74–77]. This can also be termed as “mean first passage time (MFPT)”. MFET in this context is essentially the MFPT. Furthermore, from the set of first escape times $\{\tau_{es}\}$, we directly compute the MFET $\langle \tau_{es} \rangle$ which is defined as follows,

$$\langle \tau_{es} \rangle = \int_0^{\infty} \tau_{es} F(\tau_{es}) d\tau_{es} \quad (5)$$

where $F(\tau_{es})$ is the first escape time distribution. In our simulations, to detect first escape events we continuously track the center of mass position of the nanorod, considering an escape successful when the COM position of the nanorod is outside the confinement’s boundary. We count the total number of steps taken by the nanorod to achieve the first escape and then multiply it by the simulation time. By doing so, we obtained the first escape time and by averaging all the first escape times, we computed the mean first escape time, which provides an insightful measure of the nanorod’s escape behavior in the simulations.

In Fig. 5(A), we plot $\langle \tau_{es} \rangle$ versus Pe for all three cases, confinement with single, three, and five narrow openings

($n_o = 1, 3,$ and 5). One can observe that $\langle \tau_{es} \rangle$ decreases monotonically with Pe as it is varied from 2 to 40 [78–80]. Self-propulsion always causes faster dynamics with increasing Pe , and as a result, the nanorod takes, on average, less time to reach the boundary and successfully escapes through the small open window. Higher values of Pe imply that the nanorod’s active forces are stronger compared to the random motion resulting from diffusion, as a consequence, the nanorod performs persistent motion (directed motion). We also noticed that $\langle \tau_{es} \rangle$ decreases monotonically with an increase in the number of openings on the impermeable confinement [Fig. 5(A)]. The confinement having multiple openings offers the nanorod different escape routes. If the nanorod is unable to escape through one of the exits, there is a finite probability that it will escape through the other opening(s). This multiplicity of exits significantly enhances the probability of finding a viable pathway for escape, particularly in complex or crowded environments. Furthermore, we plot $\frac{\langle \tau_{es} \rangle}{\langle \tau_{es} \rangle_{Pe=2}}$ as a function of Pe to evaluate the extent of the reduction in mean first escape time caused by activity [Fig. S6, ESI]. By comparing the values with a reference case at a specific Pe value ($Pe = 2$) for all the cases ($n_o = 1, 3, 5$), we observed a sharp decline in $\langle \tau_{es} \rangle$ as Pe increases from 2 to 5 and from 5 to 10. However, beyond Pe of 10, the reduction in $\langle \tau_{es} \rangle$ shows a relatively less pronounced difference as Pe continues to rise up to 40 [Fig. S6, ESI].

Subsequently, we depict the coefficient of variation CV (ratio of the standard deviation to the mean) in Fig. 5(B), which measures the fluctuations in the first escape times [5, 61, 76].

$$CV = \frac{\sqrt{\langle \tau_{es}^2 \rangle - \langle \tau_{es} \rangle^2}}{\langle \tau_{es} \rangle} \quad (6)$$

where $\langle \tau_{es} \rangle$ and $\langle \tau_{es}^2 \rangle$ are the first and second moments of the first escape times of a self-propelled nanorod. It is also known as “relative standard deviation”. A low CV value indicates little variation in first escape times, whereas a high CV indicates more variation. For confinement with single and three opening(s), we see an interesting non-monotonic behavior of CV as a function of Pe (Fig. 5(B)). When considering confinement with a single opening, the coefficient of variation (CV) exhibits a pattern of variation. Initially, the CV increases from $Pe = 2$ to 10 and reaches its maximum at $Pe = 10$, then decreases as Pe is further increased up to 20, then it has a small rise when Pe is increased from 20 to 40. Similarly, the CV exhibits non-monotonic behavior for a domain with three openings. In contrast, CV always increases with Pe in the case of five openings. However, CV is just a number and it is unclear how to anticipate it. In general, when CV exceeds unity, implying that the standard deviation (numerator) is greater than the mean (denom-

inator), the mean value $\langle \tau_{es} \rangle$ does not adequately represent the stochastic time scales [76]. Therefore, we must look at the full distribution $F(\tau_{es})$ of the active nanorod’s first escape times τ_{es} [Fig. 6(A-E)]. We also analyze the corresponding distribution $P(\omega)$ of the uniformity index ω [Fig. 6(F-J)], a method to quantify the trajectory-to-trajectory fluctuations in time scales [61, 74, 76], which is defined as follows,

$$\omega = \frac{\tau'_{es}}{\tau'_{es} + \tau''_{es}} \quad (7)$$

where τ'_{es} and τ''_{es} are two random first escape times for an active nanorod. It is clear from the above expression of ω , if $\tau'_{es} \gg \tau''_{es}$, $\omega \approx \frac{\tau'_{es}}{\tau'_{es}} \approx 1$. On the other hand, if $\tau'_{es} \ll \tau''_{es}$, $\omega \approx \frac{\tau'_{es}}{\tau''_{es}} \approx 0$. Interestingly, if $\tau'_{es} \approx \tau''_{es}$, $\omega \approx \frac{1}{2}$. Therefore by definition, ω varies from 0 to 1 and $\omega \approx \frac{1}{2}$, when the trajectory-to-trajectory fluctuation is minimal. In contrast, distribution $P(\omega)$ is expected to become broader and develop peaks near 0 and 1 for large fluctuations in the values of τ_{es} .

We plot $F(\tau_{es})$ and $P(\omega)$ of the first escape dynamics in Fig. 6 for various activities (Pe). Firstly, we focus on the first escape times distribution $F(\tau_{es})$ and $P(\omega)$ for the case with a single opening. For $Pe = 2$, $F(\tau_{es})$ has a broader distribution over a time scale from around 5×10^4 to 2×10^5 , where each of the trajectories has a nearly equal probability of occurring [Fig. 6(A)]. However, the distribution becomes narrower, shifts towards shorter times, and shows good exponential fittings with a larger value of β_{es} as Pe increases [Fig. 6(B-E)]. We also observe a sharper drop of $F(\tau_{es})$ with increasing Pe , which can clearly be seen from increasing value of β_{es} with Pe [Fig. 6(B-E)]. We see that at $Pe = 5$, $F(\tau_{es})$ has a typical decay over $\sim 2 \times 10^3$, but there is a sizable portion of large time data ($\tau_{es} \sim 2 \times 10^5$), which is beyond exponential fitting, as shown in Fig. 6(B). This implies that a significant fraction of the observed trajectories is short in addition to the long trajectories. We understand that most of the time, the active nanorod quickly moves toward the boundary from the center, finds a small pore, and escapes through it [see ESI, Movie S10]. On the other hand, for the same Pe , the nanorod moves along the boundary repeatedly until it gets a proper alignment towards a small opening and escapes through it [see ESI, Movie S11]. This is more prominent for $Pe = 10$, where $F(\tau_{es})$ has an initial exponential decay over a short typical time $\sim 10^3$, implying that a fraction of the observed trajectories is short, which points out that the nanorod quickly escapes [Fig. 6(C)]. One such trajectory is shown in Fig. S7(A) in ESI. Yet, in the same figure, we notice that a significant fraction of time scales are much larger ($\tau_{es} \sim 2 \times 10^5$), which is beyond exponential

fitting. This signifies that the active nanorod moves along the boundary repeatedly for an extended period of time before exiting from confinement. Such a trajectory may be seen in Fig. S7(B) in ESI. It is also reflected in the high value of CV for confinement with a single opening, $n_o = 1$ [Fig. 5(B)]. For the nanorod with higher self-propulsion (*e.g.*, $Pe = 20, 40$), $F(\tau_{es})$ displays narrower distributions with initial exponential decay over a short shorter time ($\sim 5 \times 10^2$). These fluctuations in the time scales are further supported by the behavior of $P(\omega)$.

We find that the shape of the distributions is highly dependent on Pe , as shown in Fig. 6(F-J) for confinement with a single opening. For $Pe = 2$, $P(\omega)$ represents the unimodal, bell-shaped distribution where the peak is at around $\omega = \frac{1}{2}$, indicating that most pairs of first escape times are similar and the trajectory-to-trajectory fluctuations of first escape time are not prominent. Conversely, the shape of distributions $P(\omega)$ changes on varying the activity. One can notice that $P(\omega)$ exhibits a broader distribution for $Pe = 5$. For $Pe = 10$, $P(\omega)$ shows bimodal distribution with a local minimum at around $\omega = \frac{1}{2}$ and two maxima close to $\omega = 0$ and $\omega = 1$ [Fig. 6(H)]. As discussed above, CV also has a maximum value at $Pe = 10$ [Fig. 5(B)] in the case of a single opening. This may also be seen from the snapshots of the trajectories in Fig. S7(A-B) in ESI. Moreover, the shape of $P(\omega)$ becomes increasingly broader from Fig. 6(H) to Fig. 6(J) on increasing Pe from 10 to 40. This implies, in these cases, the MFET cannot be considered an adequate measure of the actual behavior. Similar distributions have been observed earlier in experimental and theoretical studies of particles inside various confined geometries [61, 67, 74, 76]. It is important to note that the specific behavior of the fluctuations in the first escape times depends on the details of the system, the nature of self-propulsion, and the characteristics of the confinement. On the other hand, the first escape statistics exhibit large trajectory-to-trajectory fluctuation in the case of multiple openings, which is reflected in the high values of CV , the presence of multiple timescales in $F(\tau_{es})$, and multimodality in $P(\omega)$ [Fig. S8 and Fig. S9, ESI], and it is maximum for confinement with three openings at higher Pe (Fig. 5(B)). In Fig. S7(C, E) in ESI, we display short trajectories, where the nanorod quickly reaches close to the boundary and escapes for a given Pe and n_o . Whereas for the same Pe and n_o , the active nanorod moves along the circular confinement repeatedly, which results in long circular trajectories, as shown in Fig. S7(D, F) in ESI. In these cases, the MFET is not representative of the actual behavior. The presence of multiple small windows may introduce spatial heterogeneity and diverse exit pathways, which can lead to larger fluctuations in the first exit times of the active nanorod. This may be seen clearly in ESI videos, namely Movies S5, S6, S8, S9, and S12-S15, for

the confinements with multiple openings.

In addition, we compare the distributions $F(\tau_{es})$ of an active nanorod inside the confinement by varying the numbers of small openings as a function of self-propulsion [Fig. 7]. This comparative analysis enables us to understand the relationship between the number of openings, self-propulsion, and the resulting first escape times distribution for the active nanorod. From the analysis of Fig. 7, we notice a consistent trend where the distributions shift towards shorter time scales with larger values of β_{es} on increasing the number of openings for a fixed value of Pe , indicating, on average, the active nanorod takes less time to escape the confinement. As shown above in Fig. 5(B), the trajectory-to-trajectory fluctuations are more prominent for the confinement with multiple openings, as further shown in Fig. S8 and Fig. S9 in ESI. This observation suggests that the number of openings also plays a significant role in the nanorod's escape dynamics.

IV. CONCLUSION

Motivated by a growing interest in controlling the transport and diffusion of microswimmers in confined domains, we performed computer experiments to investigate the escape dynamics of a self-propelled nanorod from the circular confinements with single and multiple opening(s) through which the nanorod can escape. We repeated the simulations to obtain statistically significant information on the time taken by the nanorod to find a narrow opening and successfully exit through this. First, we simulated the passive nanorod and observed that the nanorod moves inside the circular confinement. On the other hand, our simulation results displayed that the self-driven nanorod escapes through a narrow opening due to the persistent motion if it has the orientation towards the opening and enters again through the gateway as it gets a chance. The frequency of coming out of and getting into the confinement increases with the activity as well as the number of openings on the boundary that reflects in radial probability distribution plots. For the passive case ($Pe = 0$), the probability of finding the particle inside the confinement is uniformly distributed. In contrast, in the case of the active nanorod, the probability distributions in each of the cases exhibit two peaks close to the boundary due to the faster and more persistent motion of the self-propelled nanorod. Interestingly, the radial probability density profiles become narrower with self-propulsion due to the impermeable boundary, and peaks shift more towards the confinement wall. For a deeper understanding of the escape dynamics of the active nanorod, we analyzed the mean first escape time, coefficient of variation, and uniformity index distributions. Interestingly, it has been found that the mean escape time reduces as the self-propulsion increases, as would be intuitively ex-

pected, while their fluctuations vary non-monotonically. We also observed a non-monotonic behavior by changing the number of openings within the system. We hope that our current study will help in designing self-driven nanorobots assigned to navigate through narrow channels [18, 45, 81, 82].

ACKNOWLEDGEMENTS

P. K. thanks IIT Bombay for Institute Postdoctoral Fellowship. R. C. acknowledges Science and Engineering Research Board (SERB) for funding (Project No. MTR/2020/000230 under MATRICS scheme) for funding. We acknowledge the SpaceTime-2 supercomputing facility at IIT Bombay for the computing time. P. K. would like to thank Dr. Koushik Goswami and Rajiblochan Sahoo for critically reading the manuscript and discussing it.

DATA AVAILABILITY

The data that supports the findings of this study are available within the article [and its supplementary material].

SUPPLEMENTARY MATERIAL

The method and parameter validation is carried out for a nanorod in free space. The translational $\left(\langle \Delta r_c^2(\tau) \rangle\right)$ mean square displacement is calculated. From the plot (Fig. S1) for $Pe = 0$, we have computed the thermal translational diffusion coefficient, $D_T = 1.87 \times 10^{-5}$ and friction coefficient, $\gamma = 5.33 \times 10^4$.

Movies

Movie_S1: Brownian dynamics simulation of the passive ($Pe = 0$) nanorod for the confinement with a single narrow opening ($n_o = 1$).

Movie_S2: Brownian dynamics simulation of the passive ($Pe = 0$) nanorod for the confinement with three narrow openings ($n_o = 3$).

Movie_S3: Brownian dynamics simulation of the passive ($Pe = 0$) nanorod for the confinement with five narrow openings ($n_o = 5$).

Movie_S4: Brownian dynamics simulation of the active ($Pe = 5$) nanorod for the confinement with a single narrow opening ($n_o = 1$).

Movie_S5: Brownian dynamics simulation of the active ($Pe = 5$) nanorod for the confinement with three narrow openings ($n_o = 3$).

Movie_S6: Brownian dynamics simulation of the active ($Pe = 5$) nanorod for the confinement with five narrow openings ($n_o = 5$).

Movie_S7: Brownian dynamics simulation of the active ($Pe = 20$) nanorod for the confinement with a single nar-

row opening ($n_o = 1$).

Movie_S8: Brownian dynamics simulation of the active ($Pe = 20$) nanorod for the confinement with three narrow openings ($n_o = 3$).

Movie_S9: Brownian dynamics simulation of the active ($Pe = 20$) nanorod for the confinement with five narrow openings ($n_o = 5$).

Movie_S10: Brownian dynamics simulation of the active ($Pe = 10$) nanorod for the confinement with a single narrow opening ($n_o = 1$). Here, the active nanorod quickly moves toward the boundary from the center, finds a small pore, and escapes through it.

Movie_S11: Brownian dynamics simulation of the active ($Pe = 10$) nanorod for the confinement with a single narrow opening ($n_o = 1$). The active nanorod moves along the boundary repeatedly for a long time.

Movie_S12: Brownian dynamics simulation of the active ($Pe = 5$) nanorod for the confinement with three narrow openings ($n_o = 3$). Here, the nanorod has a small trajectory.

Movie_S13: Brownian dynamics simulation of the active ($Pe = 5$) nanorod for the confinement with three narrow openings ($n_o = 3$). Here, the active nanorod moves along the boundary repeatedly for a long time, it has a long circular trajectory.

Movie_S14: Brownian dynamics simulation of the active ($Pe = 40$) nanorod for the confinement with five narrow openings ($n_o = 5$). Here, the active nanorod quickly escapes through a narrow opening.

Movie_S15: Brownian dynamics simulation of the active ($Pe = 40$) nanorod for the confinement with five narrow openings ($n_o = 5$). The active nanorod moves along the boundary repeatedly for a long time to escape from the confinement.

For the passive case ($Pe = 0$), $\langle \Delta r_c^2(\tau) \rangle$ is always diffusive $\left(\langle \Delta r_c^2(\tau) \rangle \sim \tau\right)$ with the diffusion coefficient D_T .

In case of the self-propelled nanorod, $\langle \Delta r_c^2(\tau) \rangle$ exhibits three distinct regions: diffusive at short time, superdiffusive region at the intermediate time which scales as $\langle \Delta r_c^2(\tau) \rangle \sim \tau^2$. At longer time, $\langle \Delta r_c^2(\tau) \rangle$ becomes linear in time with an enhanced diffusion coefficient.

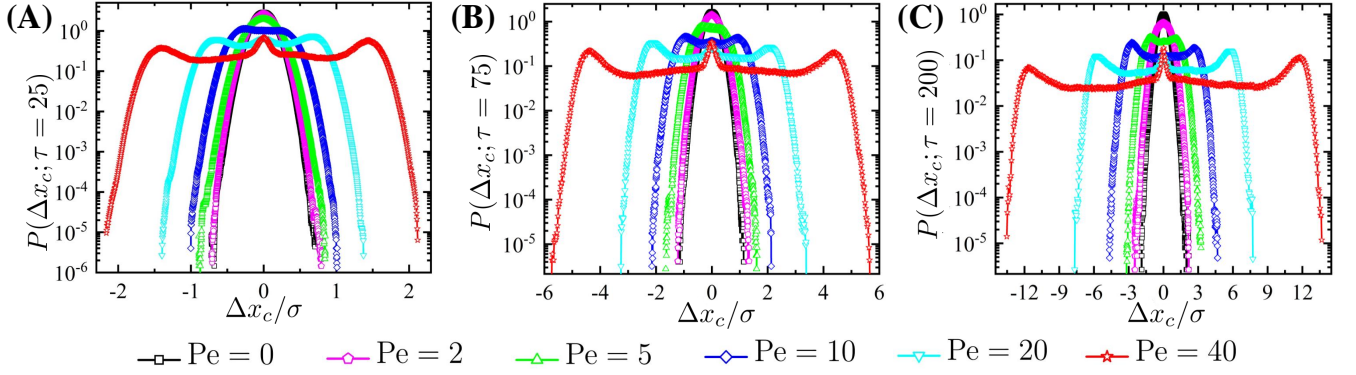


Fig. 4. Plots (A)-(C) represent displacement distribution functions $P(\Delta x_c; \tau)$ of a nanorod at different lag times $\tau = 25, 75, 200$ for the confinement with three narrow openings.

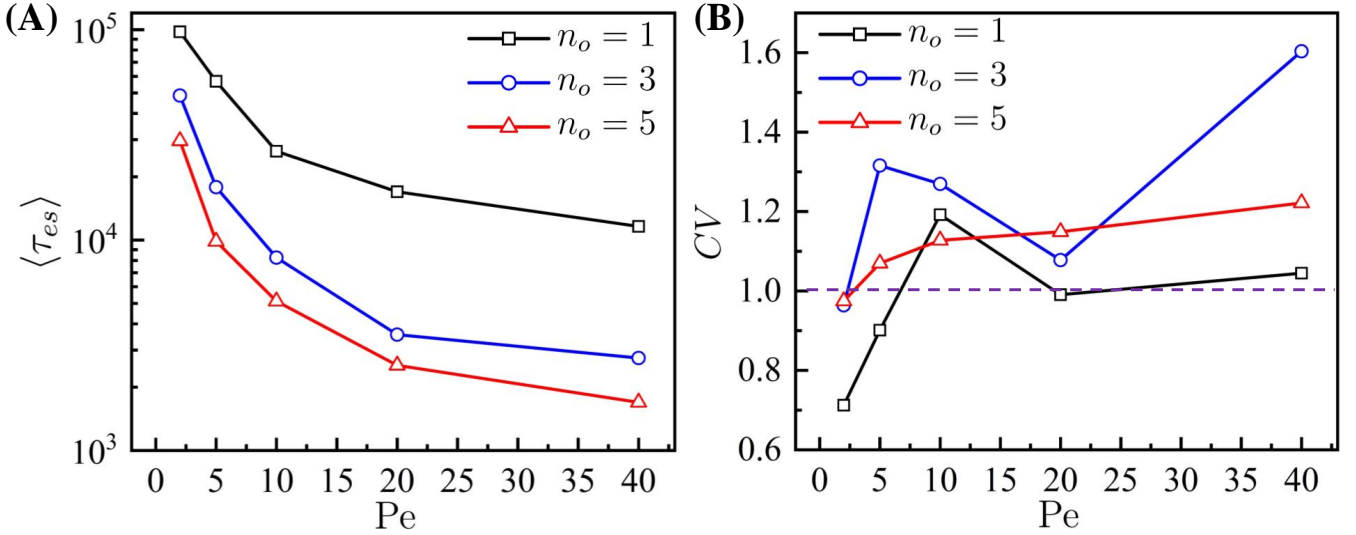


Fig. 5. Plot of (A) mean first escape time (MFET) $\langle \tau_{es} \rangle$ and (B) coefficient of variation (CV) versus Pe. Here, one can observe the monotonic decrease of $\langle \tau_{es} \rangle$ with an increase in Pe and the non-monotonic change of CV as a function of Pe.

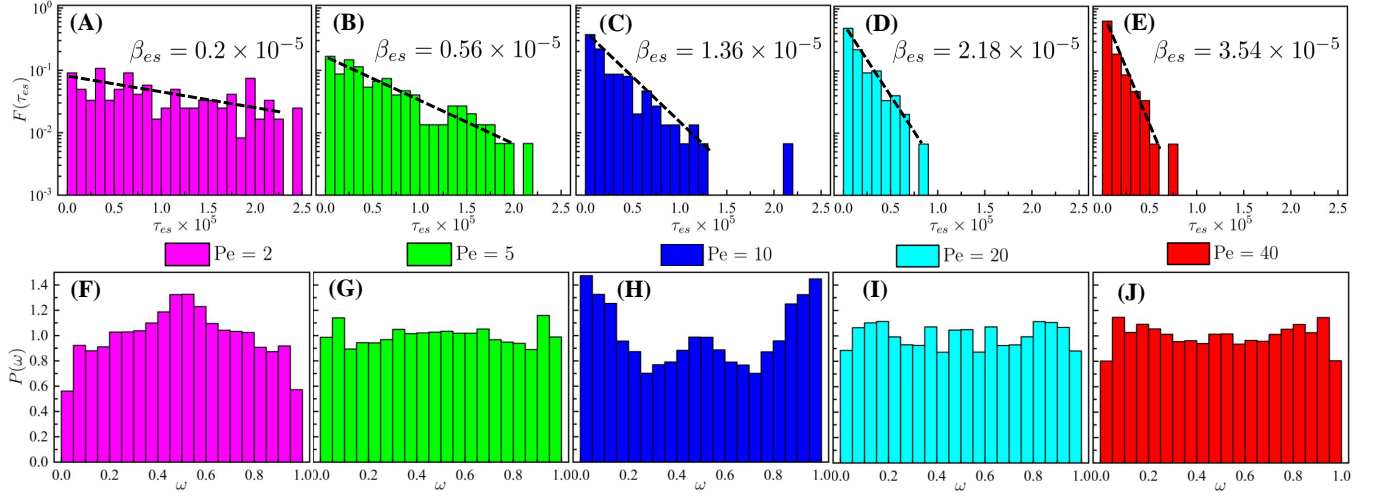


Fig. 6. Plots of the first escape times distributions $F(\tau_{es})$ and corresponding uniformity index distributions $P(\omega)$ of self-driven nanorod are shown in (A-E) and (F-J), respectively, at $Pe = 2, 5, 10, 20, 40$, for confinement with a single window. $P(\omega)$ has a unimodal behavior at the lowest values of $Pe = 2$, but not for higher values of Pe . One can see that a significant fraction of large-time data is beyond short-time exponential fittings.

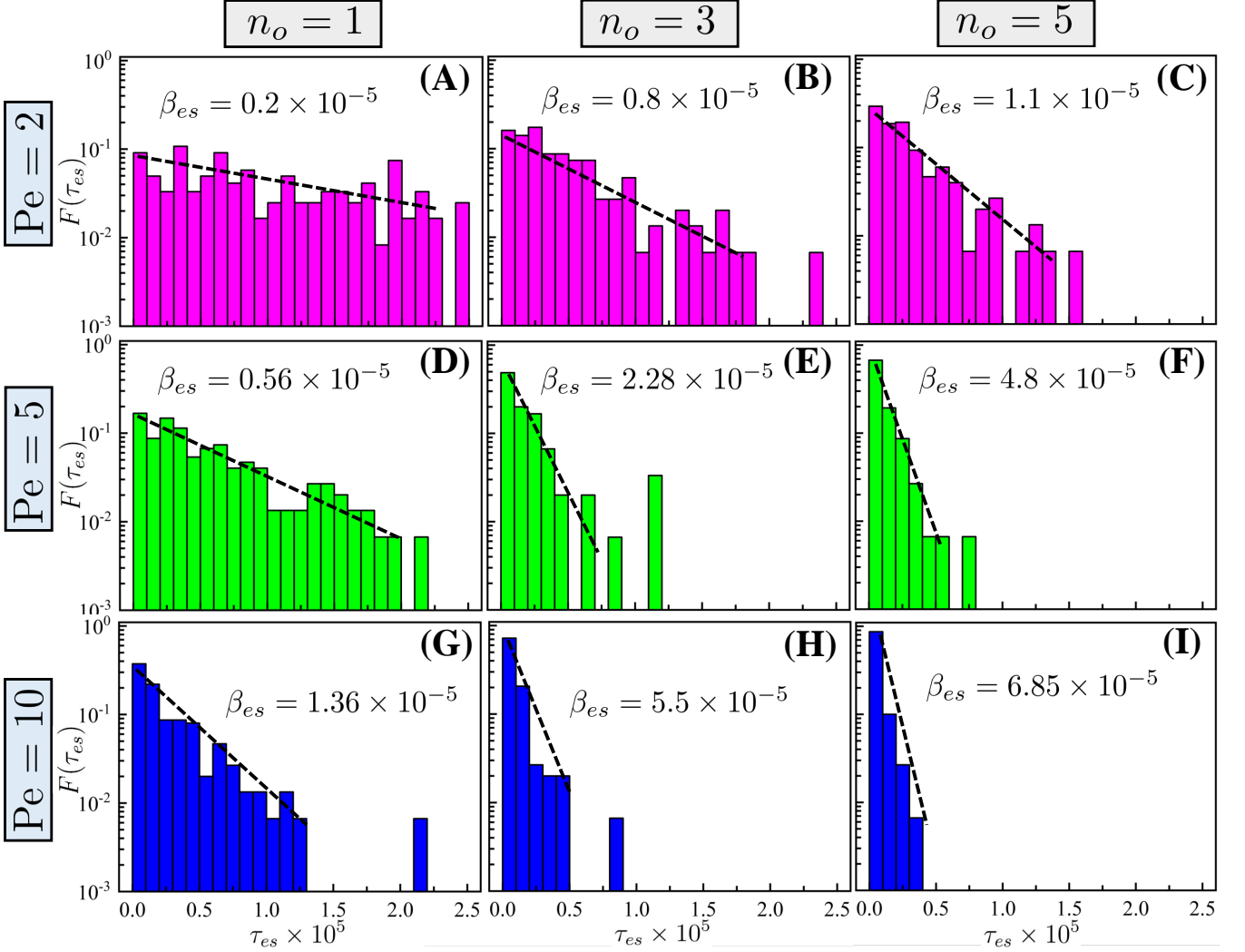


Fig. 7. A comparison of $F(\tau_{es})$ for different values of Pe (from top to bottom for a given value of n_o) and the number of openings n_o (from left to right for a given value of Pe). We see a significant fraction of τ_{es} shifts towards shorter times on increasing Pe and n_o . Short to moderate time data show good exponential fittings and the slope β_{es} increases with activity (Pe) and n_o .

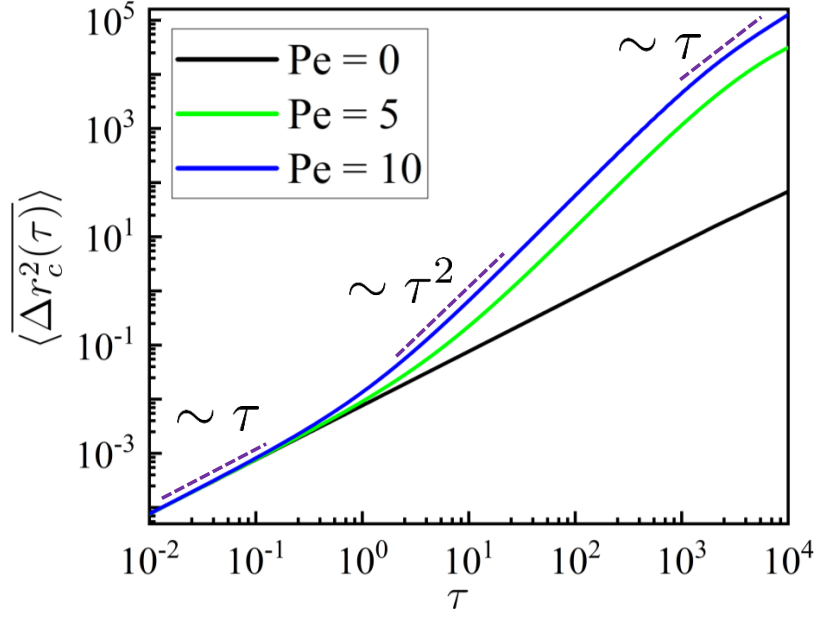


Fig. S1. Log-log plot of $\langle \Delta r_c^2(\tau) \rangle$ for the self-propelled nanorod at different Pe.

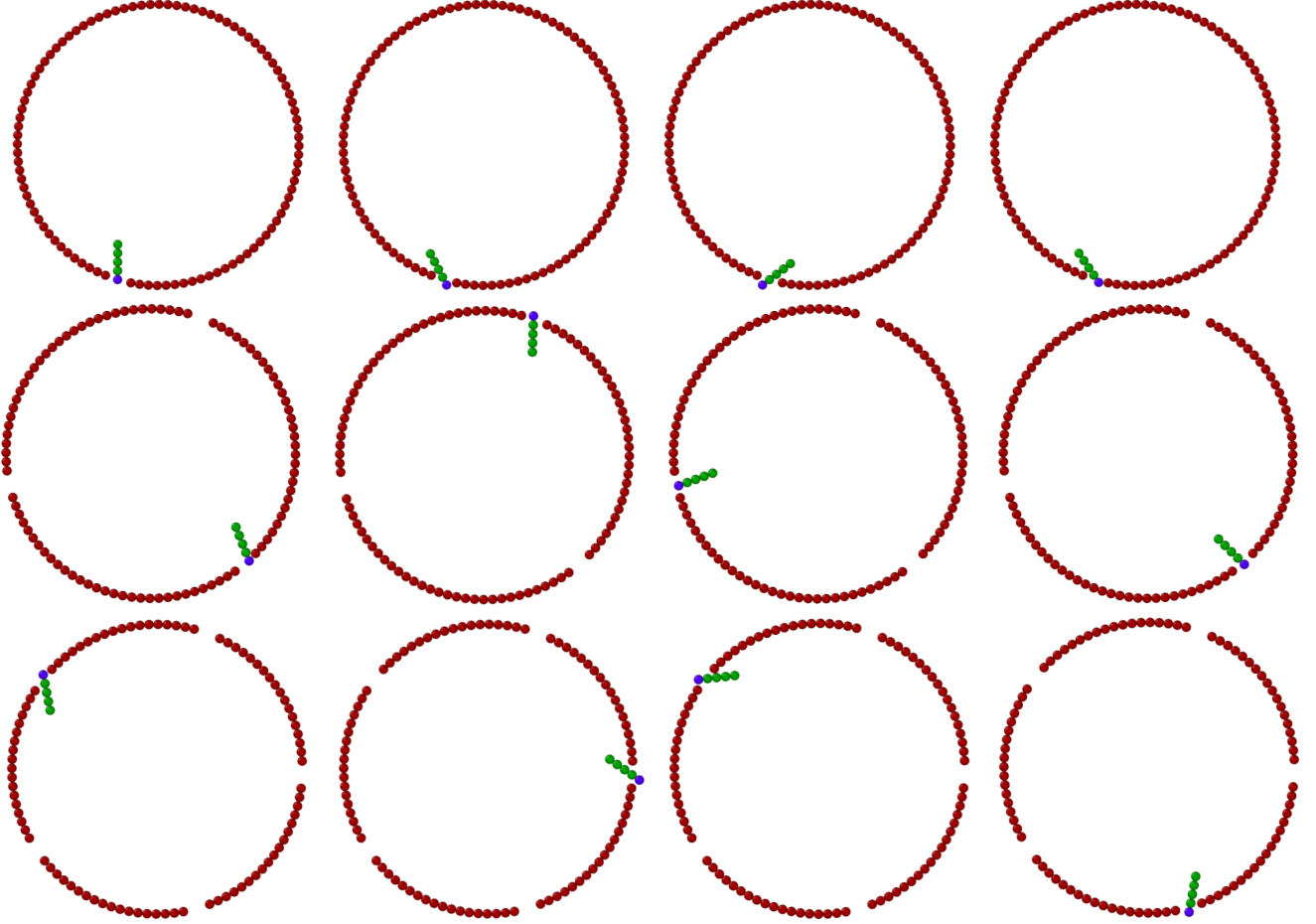


Fig. S2. Here are some snapshots from the simulations where the nanorod successfully escapes through the narrow opening(s) with different orientations.

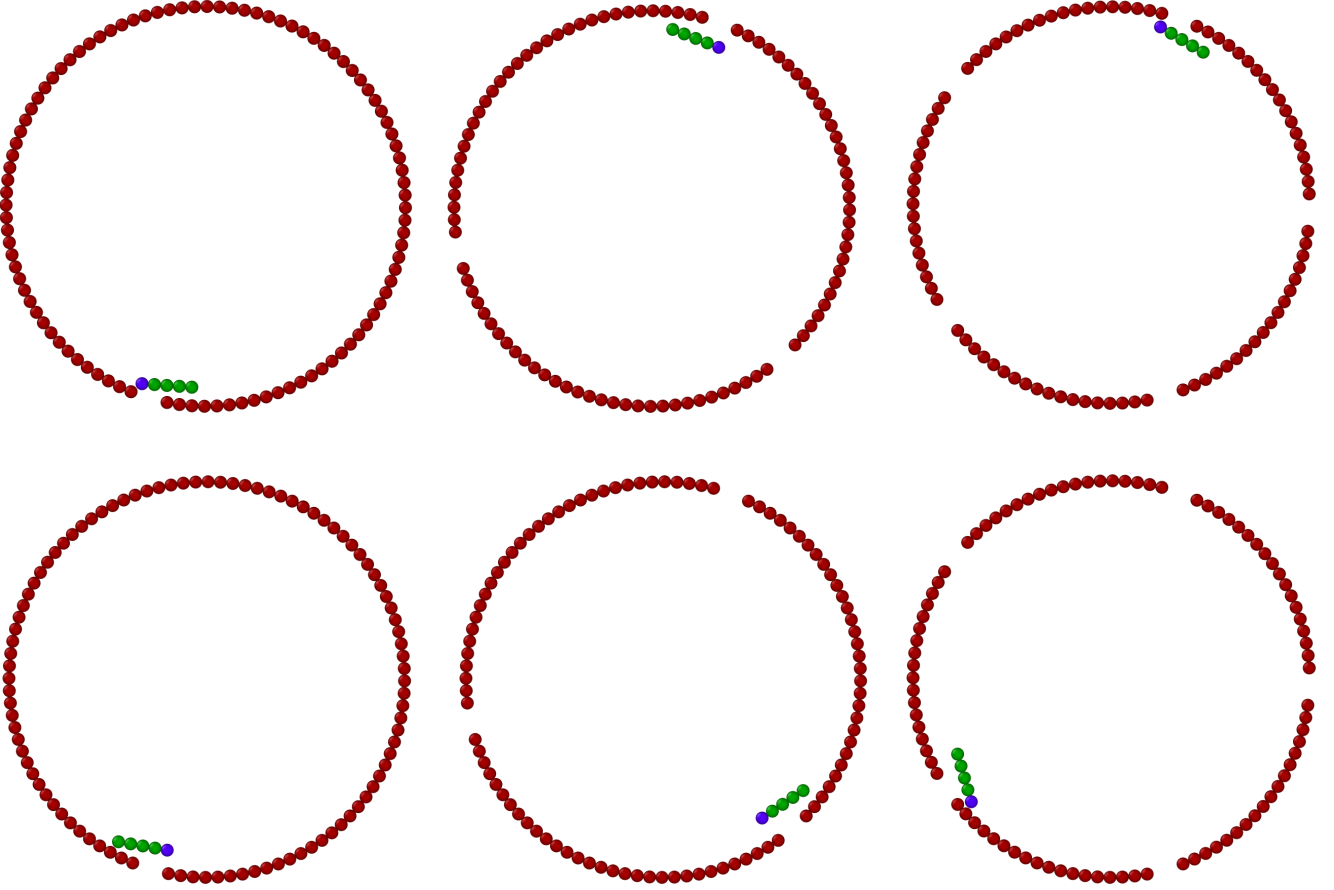


Fig. S3. Here are some snapshots from the simulations depicting instances where the nanorod is unable to escape through the narrow opening(s) due to its improper orientation as it remains nearly parallel to the wall.

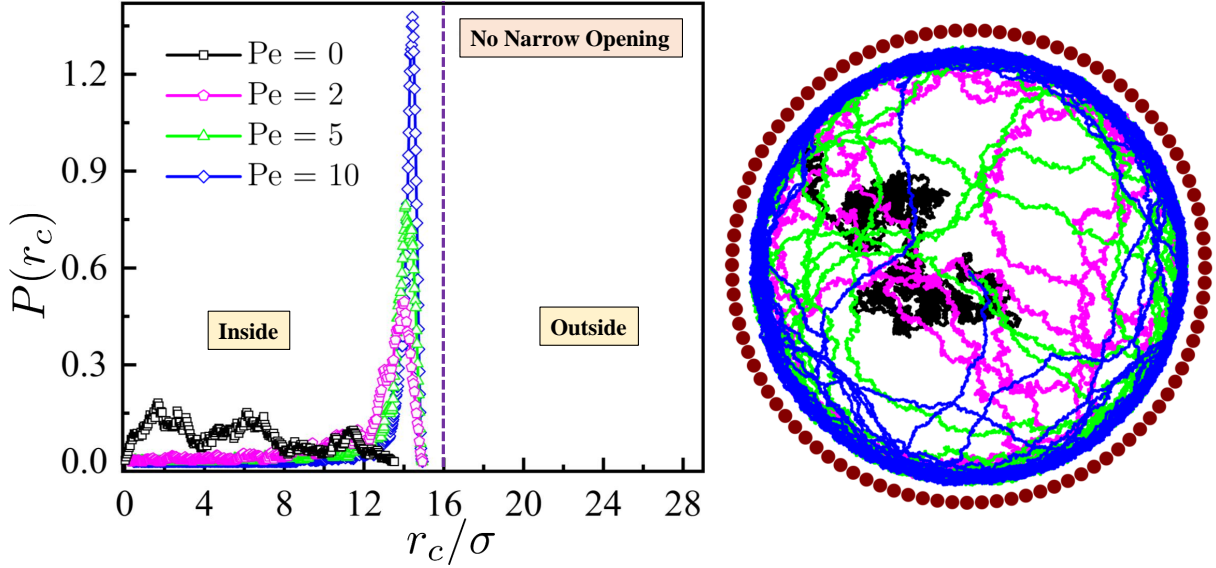


Fig. S4. The radial probability distributions $P(r_c)$ of the nanorod for the confinement without opening, $n_o = 0$ (left) and the corresponding COM trajectories (right) for different Pe .

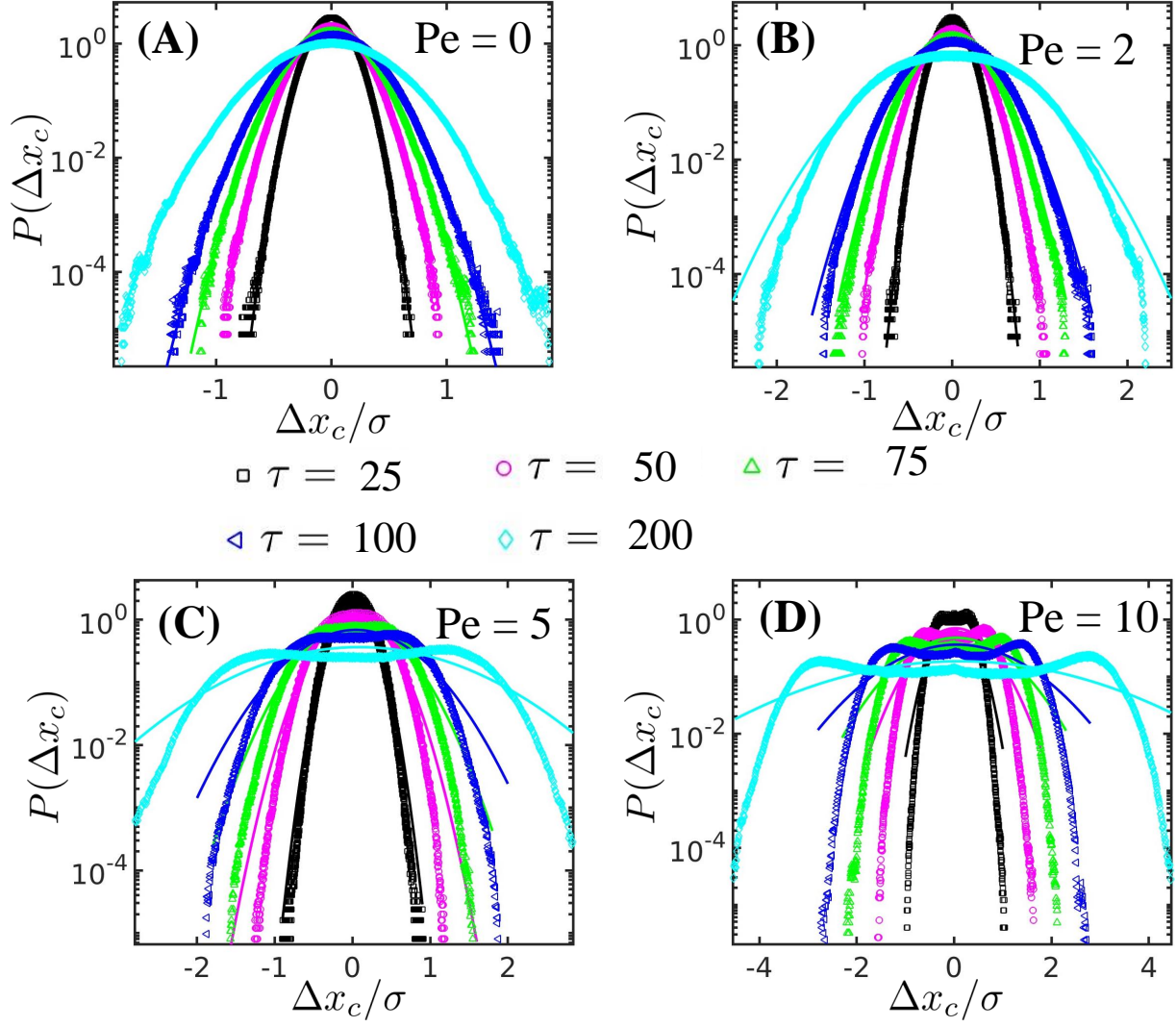


Fig. S5. Plots (A)-(D) represent displacement distribution functions $P(\Delta x_c)$ of a nanorod at different lag times $\tau = 25, 50, 75, 100, 200$ for the confinement with three narrow openings. Solid lines represent the Gaussian fittings.

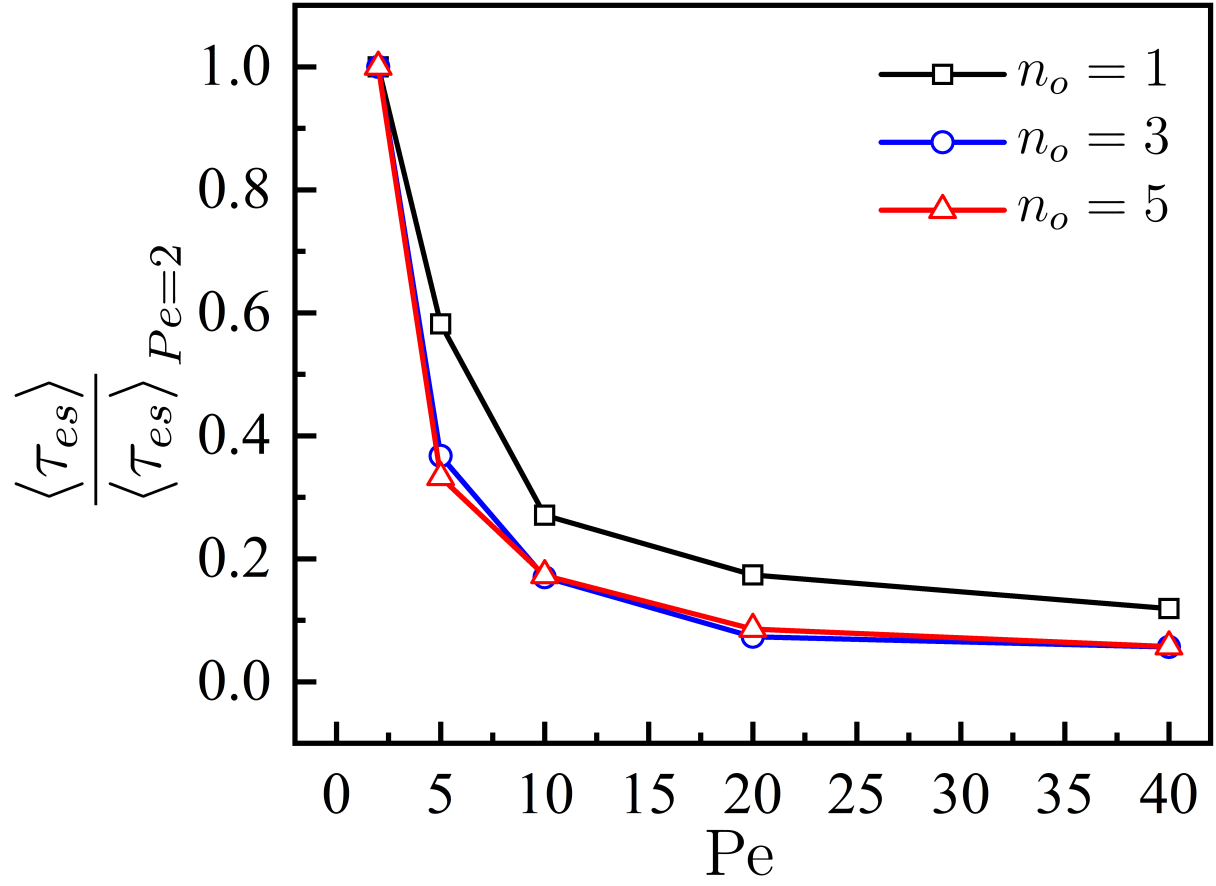


Fig. S6. Plot of $\frac{\langle \tau_{es} \rangle}{\langle \tau_{es} \rangle_{Pe=2}}$ versus Pe .

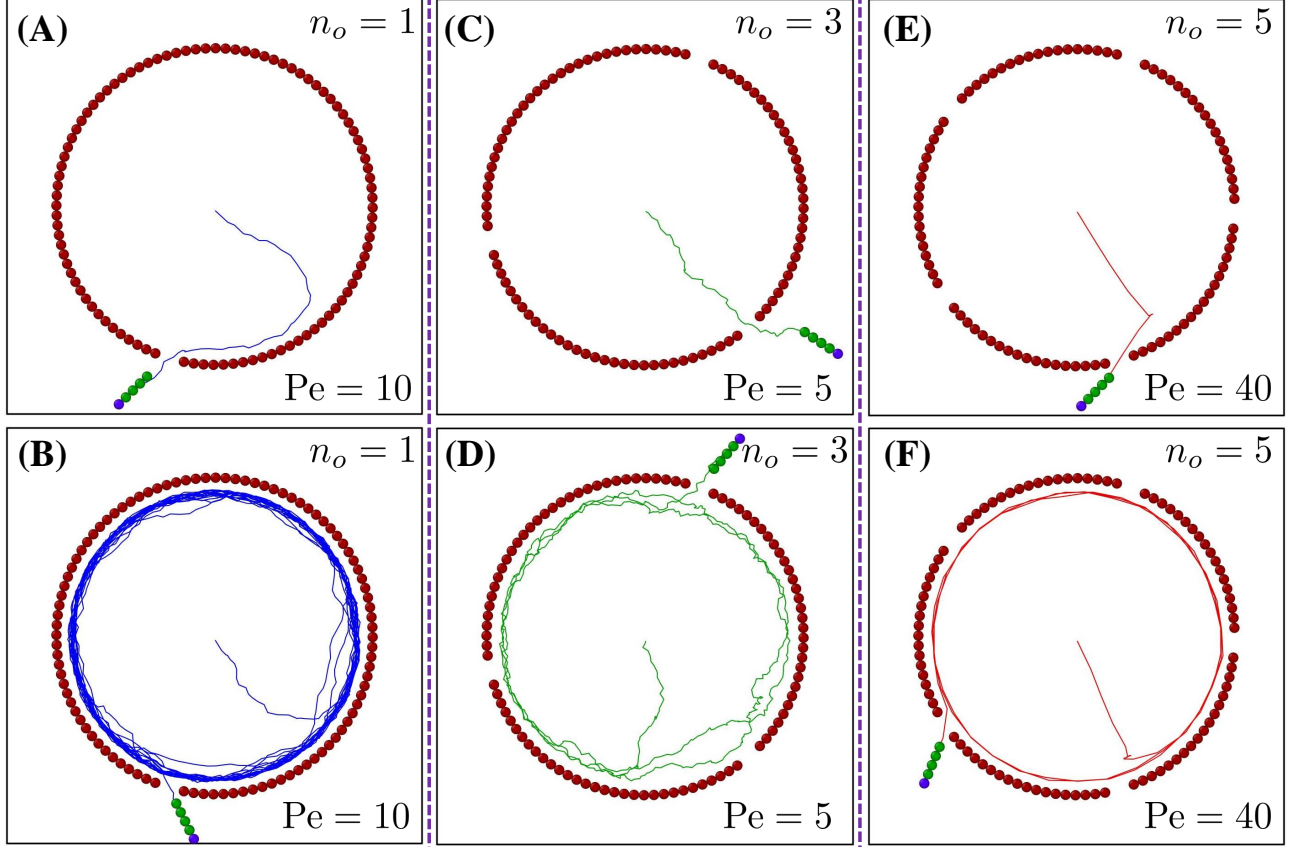


Fig. S7. The COM trajectories of the nanorod in (A) short time escape trajectory, (B) long time escape trajectory at $Pe = 10$ for a single opening case, (C) short time escape trajectory, (D) long time escape trajectory at $Pe = 5$ for three openings case, (E) short time escape trajectory, and (F) long time escape trajectory at $Pe = 40$ for five openings case

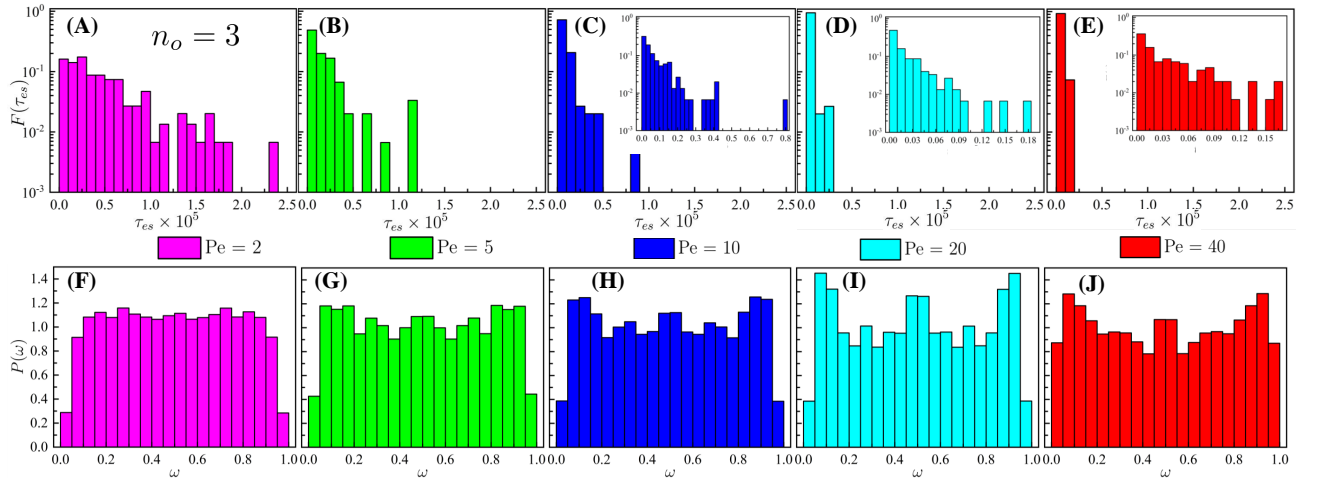


Fig. S8. Plots of the first escape times distributions $F(\tau_{es})$ and corresponding uniformity index distributions $P(\omega)$ of self-driven nanorod are shown in (A-E) and (F-J), respectively, at $Pe = 2, 5, 10, 20, 40$, for confinement with three openings.

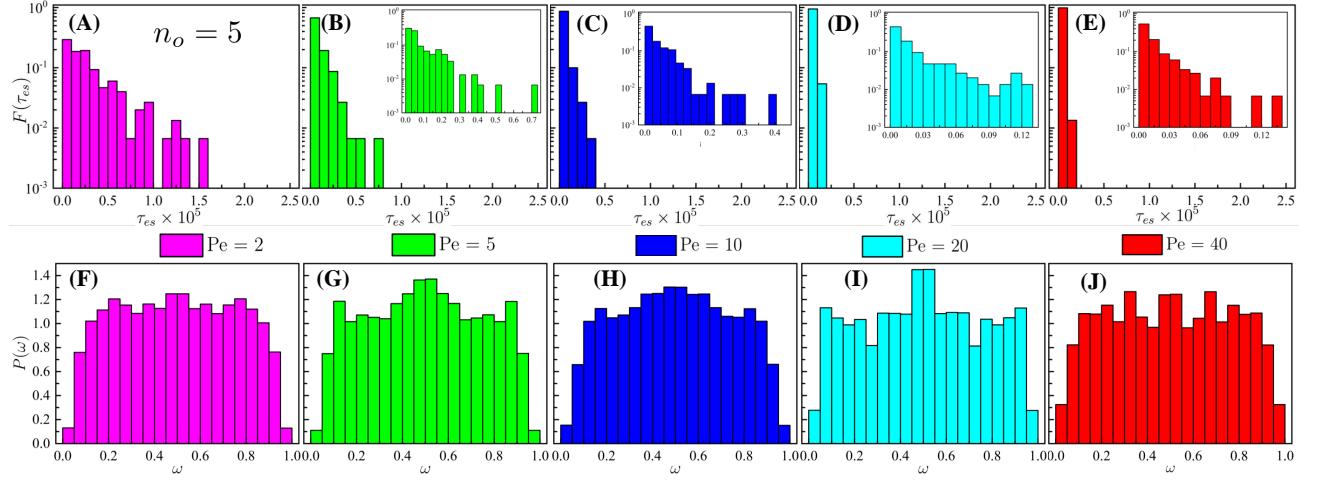


Fig. S9. Plots of the first escape times distributions $F(\tau_{es})$ and corresponding uniformity index distributions $P(\omega)$ of self-driven nanorod are shown in (A-E) and (F-J), respectively, at $Pe = 2, 5, 10, 20, 40$, for confinement with five openings.

- [1] Z. Schuss, A. Singer, and D. Holcman, The narrow escape problem for diffusion in cellular microdomains, *Proc. Natl. Acad. Sci. U.S.A.* **104**, 16098 (2007).
- [2] P. C. Bressloff and J. M. Newby, Stochastic models of intracellular transport, *Rev. Mod. Phys.* **85**, 135 (2013).
- [3] D. Holcman and Z. Schuss, *Stochastic narrow escape in molecular and cellular biology, Analysis and Applications*. Springer, New York **48**, 108 (2015).
- [4] I. V. Grigoriev, Y. A. Makhnovskii, A. M. Berezhkovskii, and V. Y. Zitserman, Kinetics of escape through a small hole, *J. Chem. Phys.* **116**, 9574 (2002).
- [5] A. D. Co, M. C. Lagomarsino, M. Caselle, and M. Osella, Stochastic timing in gene expression for simple regulatory strategies, *Nucleic Acids Res.* **45**, 1069 (2017).
- [6] S. A. Gorski, M. Dundr, and T. Misteli, The road much traveled: trafficking in the cell nucleus, *Curr. Opin. Cell Biol.* **18**, 284 (2006).
- [7] T. Misteli, Physiological importance of rna and protein mobility in the cell nucleus, *Histochem. Cell Biol.* **129**, 5 (2008).
- [8] C. Loverdo, O. Bénichou, M. Moreau, and R. Voituriez, Enhanced reaction kinetics in biological cells, *Nat. Phys.* **4**, 134 (2008).
- [9] P. Chopra, D. Quint, A. Gopinathan, and B. Liu, Geometric effects induce anomalous size-dependent active transport in structured environments, *Phys. Rev. Fluids* **7**, L071101 (2022).
- [10] L. Theeyancheri, S. Chaki, T. Bhattacharjee, and R. Chakrabarti, Migration of active rings in porous media, *Phys. Rev. E* **106**, 014504 (2022).
- [11] M. Muthukumar, Polymer translocation through a hole, *J. Chem. Phys.* **111**, 10371 (1999).
- [12] K. L. Sebastian and A. K. Paul, Kramers problem for a polymer in a double well, *Phys. Rev. E* **62**, 927 (2000).
- [13] K. Chen, I. Jou, N. Ermann, M. Muthukumar, U. F. Keyser, and N. A. Bell, Dynamics of driven polymer transport through a nanopore, *Nat. Phys.* **17**, 1043 (2021).
- [14] O. Bénichou and R. Voituriez, Narrow-escape time problem: time needed for a particle to exit a confining domain through a small window, *Phys. Rev. Lett.* **100**, 168105 (2008).
- [15] D. S. Grebenkov and G. Oshanin, Diffusive escape through a narrow opening: new insights into a classic problem, *Phys. Chem. Chem. Phys.* **19**, 2723 (2017).
- [16] V. Srivastava and A. Cheviakov, Brownian dynamics simulations for the narrow escape problem in the unit sphere, *Phys. Rev. E* **104**, 064113 (2021).
- [17] S. Behzadi, V. Serpooshan, W. Tao, M. A. Hamaly, M. Y. Alkawareek, E. C. Dreaden, D. Brown, A. M. Alkilany, O. C. Farokhzad, and M. Mahmoudi, Cellular uptake of nanoparticles: journey inside the cell, *Chem. Soc. Rev.* **46**, 4218 (2017).
- [18] M. J. Mitchell, M. M. Billingsley, R. M. Haley, M. E. Wechsler, N. A. Peppas, and R. Langer, Engineering precision nanoparticles for drug delivery, *Nat. Rev. Drug Discov.* **20**, 101 (2021).
- [19] P. S. Burada, P. Hänggi, F. Marchesoni, G. Schmid, and P. Talkner, Diffusion in confined geometries, *ChemPhysChem* **10**, 45 (2009).
- [20] L. Bosi, P. K. Ghosh, and F. Marchesoni, Analytical estimates of free brownian diffusion times in corrugated narrow channels, *J. Chem. Phys.* **137**, 174110 (2012).
- [21] P. Hänggi and F. Marchesoni, Artificial brownian motors: Controlling transport on the nanoscale, *Rev. Mod. Phys.* **81**, 387 (2009).
- [22] L. Kullman, M. Winterhalter, and S. M. Bezrukov, Transport of maltodextrins through maltoporin: a single-channel study, *Biophys. J.* **82**, 803 (2002).
- [23] A. Biess, E. Korkotian, and D. Holcman, Diffusion in a dendritic spine: the role of geometry, *Phys. Rev. E* **76**, 021922 (2007).
- [24] T. Agranov and B. Meerson, Narrow escape of interacting diffusing particles, *Phys. Rev. Lett.* **120**, 120601 (2018).
- [25] D. S. Grebenkov, R. Metzler, and G. Oshanin, Full distribution of first exit times in the narrow escape problem, *New J. Phys.* **21**, 122001 (2019).
- [26] P. K. Ghosh, R. Glavey, F. Marchesoni, S. E. Savel'ev, and F. Nori, Geometric stochastic resonance in a double cavity, *Phys. Rev. E* **84**, 011109 (2011).
- [27] C. Chevalier, O. Bénichou, B. Meyer, and R. Voituriez, First-passage quantities of brownian motion in a bounded domain with multiple targets: a unified approach, *J. Phys. A: Math. Theor.* **44**, 025002 (2011).
- [28] P. Bressloff and B. Earnshaw, Diffusion-trapping model of receptor trafficking in dendrites, *Phys. Rev. E* **75**, 041915 (2007).
- [29] D. Holcman and Z. Schuss, Escape through a small opening: receptor trafficking in a synaptic membrane, *J. Stat. Phys.* **117**, 975 (2004).
- [30] D. Freche, U. Pannasch, N. Rouach, and D. Holcman, Synapse geometry and receptor dynamics modulate synaptic strength, *PloS One* **6**, e25122 (2011).
- [31] H. Chen and F. Huang, First passage of a diffusing particle under stochastic resetting in bounded domains with spherical symmetry, *Phys. Rev. E* **105**, 034109 (2022).
- [32] C. Bechinger, R. Di Leonardo, H. Löwen, C. Reichardt, G. Volpe, and G. Volpe, Active particles in complex and crowded environments, *Rev. Mod. Phys.* **88**, 045006 (2016).
- [33] L. Theeyancheri, R. Sahoo, P. Kumar, and R. Chakrabarti, In silico studies of active probe dynamics in crowded media, *ACS Omega* **7**, 33637 (2022).
- [34] L. Theeyancheri, S. Chaki, T. Bhattacharjee, and R. Chakrabarti, Active dynamics of linear chains and rings in porous media, *J. Chem. Phys.* **159**, 014902 (2023).
- [35] P. Kumar and R. Chakrabarti, Dynamics of self-propelled tracer particles inside a polymer network, *Phys. Chem. Chem. Phys.* **25**, 1937 (2023).
- [36] N. Narinder, J. R. Gomez-Solano, and C. Bechinger, Active particles in geometrically confined viscoelastic fluids, *New J. Phys.* **21**, 093058 (2019).
- [37] L. Caprini and U. M. B. Marconi, Active particles under confinement and effective force generation among surfaces, *Soft Matter* **14**, 9044 (2018).
- [38] T. Jakuszeit, O. A. Croze, and S. Bell, Diffusion of active particles in a complex environment: role of surface scattering, *Phys. Rev. E* **99**, 012610 (2019).
- [39] O. Chepizhko and F. Peruani, Diffusion, subdiffusion, and trapping of active particles in heterogeneous media,

- Phys. Rev. Lett. **111**, 160604 (2013).
- [40] P. K. Ghosh, F. Marchesoni, Y. Li, and F. Nori, Active particle diffusion in convection roll arrays, Phys. Chem. Chem. Phys. **23**, 11944 (2021).
- [41] L. Caprini, F. Cecconi, A. Puglisi, and A. Sarracino, Diffusion properties of self-propelled particles in cellular flows, Soft Matter **16**, 5431 (2020).
- [42] S. Nayak, T. Debnath, S. Das, D. Debnath, and P. K. Ghosh, Escape kinetics of an underdamped colloidal particle from a cavity through narrow pores, J. Phys. Chem. C **124**, 18747 (2020).
- [43] T. Debnath, P. Chaudhury, T. Mukherjee, D. Mondal, and P. K. Ghosh, Escape kinetics of self-propelled particles from a circular cavity, J. Chem. Phys. **155**, 194102 (2021).
- [44] S. Ramaswamy, The mechanics and statistics of active matter, Annu. Rev. Condens. Matter Phys. **1**, 323 (2010).
- [45] J. Mujtaba, J. Liu, K. K. Dey, T. Li, R. Chakraborty, K. Xu, D. Makarov, R. A. Barmin, D. A. Gorin, V. P. Tolstoy, *et al.*, Micro-bio-chemo-mechanical-systems: Micromotors, microfluidics, and nanozymes for biomedical applications, Adv. Mater. **33**, 2007465 (2021).
- [46] H.-P. Zhang, A. Be'er, E.-L. Florin, and H. L. Swinney, Collective motion and density fluctuations in bacterial colonies, Proc. Natl. Acad. Sci. U.S.A. **107**, 13626 (2010).
- [47] A. Sokolov, I. S. Aranson, J. O. Kessler, and R. E. Goldstein, Concentration dependence of the collective dynamics of swimming bacteria, Phys. Rev. Lett. **98**, 158102 (2007).
- [48] L. J. Fauci and R. Dillon, Biofluidmechanics of reproduction, Annu. Rev. Fluid Mech. **38**, 371 (2006).
- [49] J. Buhl, D. J. Sumpter, I. D. Couzin, J. J. Hale, E. Despland, E. R. Miller, and S. J. Simpson, From disorder to order in marching locusts, Science **312**, 1402 (2006).
- [50] K. Tunström, Y. Katz, C. C. Ioannou, C. Huepe, M. J. Lutz, and I. D. Couzin, Collective states, multistability and transitional behavior in schooling fish, PLoS Comput. Biol. **9**, e1002915 (2013).
- [51] A. Kudrolli, G. Lumay, D. Volfson, and L. S. Tsimring, Swarming and swirling in self-propelled polar granular rods, Phys. Rev. Lett. **100**, 058001 (2008).
- [52] H.-R. Jiang, N. Yoshinaga, and M. Sano, Active motion of a janus particle by self-thermophoresis in a defocused laser beam, Phys. Rev. Lett. **105**, 268302 (2010).
- [53] A. M. Pourrahimi and M. Pumera, Multifunctional and self-propelled spherical janus nano/micromotors: recent advances, Nanoscale **10**, 16398 (2018).
- [54] A. Walther and A. H. Müller, Janus particles: synthesis, self-assembly, physical properties, and applications, Chem. Rev. **113**, 5194 (2013).
- [55] J. Ignés-Mullol and F. Sagués, Experiments with active and driven synthetic colloids in complex fluids, Curr. Opin. Colloid Interface Sci. , 101636 (2022).
- [56] J. Palacci, S. Sacanna, A. P. Steinberg, D. J. Pine, and P. M. Chaikin, Living crystals of light-activated colloidal surfers, Science **339**, 936 (2013).
- [57] R. Kapral, Perspective: Nanomotors without moving parts that propel themselves in solution, J. Chem. Phys. **138**, 020901 (2013).
- [58] J. R. Howse, R. A. Jones, A. J. Ryan, T. Gough, R. Vafabakhsh, and R. Golestanian, Self-motile colloidal particles: from directed propulsion to random walk, Phys. Rev. Lett. **99**, 048102 (2007).
- [59] I. Buttinoni, J. Bialké, F. Kümmel, H. Löwen, C. Bechinger, and T. Speck, Dynamical clustering and phase separation in suspensions of self-propelled colloidal particles, Phys. Rev. Lett. **110**, 238301 (2013).
- [60] Y. Fily and M. C. Marchetti, Athermal phase separation of self-propelled particles with no alignment, Phys. Rev. Lett. **108**, 235702 (2012).
- [61] A. Biswas, J. Cruz, P. Parmananda, and D. Das, First passage of an active particle in the presence of passive crowdsters, Soft Matter **16**, 6138 (2020).
- [62] P. K. Ghosh, Communication: Escape kinetics of self-propelled janus particles from a cavity: Numerical simulations, J. Chem. Phys. **141**, 061102 (2014).
- [63] L. Caprini, F. Cecconi, and U. Marini Bettolo Marconi, Transport of active particles in an open-wedge channel, J. Chem. Phys. **150**, 144903 (2019).
- [64] M. Khatami, K. Wolff, O. Pohl, M. R. Ejtehadi, and H. Stark, Active brownian particles and run-and-tumble particles separate inside a maze, Sci. Rep. **6**, 1 (2016).
- [65] K. S. Olsen, L. Angheluta, and E. G. Flekkøy, Escape problem for active particles confined to a disk, Phys. Rev. Res. **2**, 043314 (2020).
- [66] M. Paoluzzi, L. Angelani, and A. Puglisi, Narrow-escape time and sorting of active particles in circular domains, Phys. Rev. E **102**, 042617 (2020).
- [67] A. Biswas and A. Kudrolli, Escape dynamics of confined undulating worms, Soft Matter **19**, 4376 (2023).
- [68] T. Lagache and D. Holcman, Extended narrow escape with many windows for analyzing viral entry into the cell nucleus, J. Stat. Phys. **166**, 244 (2017).
- [69] S. Condamin, O. Bénichou, and M. Moreau, First-passage times for random walks in bounded domains, Phys. Rev. Lett. **95**, 260601 (2005).
- [70] A. Stukowski, Visualization and analysis of atomistic simulation data with ovito—the open visualization tool, Modelling Simul. Mater. Sci. Eng. **18**, 015012 (2010).
- [71] J. D. Weeks, D. Chandler, and H. C. Andersen, Role of repulsive forces in determining the equilibrium structure of simple liquids, J. Chem. Phys. **54**, 5237 (1971).
- [72] S. Plimpton, Fast parallel algorithms for short-range molecular dynamics, J. Comp. Phys. **117**, 1 (1995).
- [73] P. Kumar, L. Theeyancheri, and R. Chakrabarti, Chemically symmetric and asymmetric self-driven rigid dumbbells in a 2d polymer gel, Soft Matter **18**, 2663 (2022).
- [74] T. G. Mattos, C. Mejía-Monasterio, R. Metzler, G. Oshanin, and G. Schehr, Trajectory-to-trajectory fluctuations in first-passage phenomena in bounded domains, in *First-Passage Phenomena and Their Applications* (World Scientific, 2014) pp. 203–225.
- [75] C. Mejía-Monasterio, G. Oshanin, and G. Schehr, First passages for a search by a swarm of independent random searchers, J. Stat. Mech. **2011**, P06022 (2011).
- [76] T. G. Mattos, C. Mejía-Monasterio, R. Metzler, and G. Oshanin, First passages in bounded domains: When is the mean first passage time meaningful?, Phys. Rev. E **86**, 031143 (2012).
- [77] R. Chakrabarti and K. L. Sebastian, A lower bound to the survival probability and an approximate first passage time distribution for markovian and non-markovian dynamics in phase space, J. Chem. Phys. **131**, 224504 (2009).
- [78] L. Caprini, F. Cecconi, and U. Marini Bettolo Marconi, Correlated escape of active particles across a potential barrier, J. Chem. Phys. **155**, 234902 (2021).
- [79] S. Chaki and R. Chakrabarti, Escape of a passive particle

- from an activity-induced energy landscape: emergence of slow and fast effective diffusion, *Soft Matter* **16**, 7103 (2020).
- [80] K. Goswami and R. Metzler, Effects of active noise on transition-path dynamics, *J. Phys. Complex.* **4**, 025005 (2023).
- [81] M. Medina-Sánchez, H. Xu, and O. G. Schmidt, Micro- and nano-motors: the new generation of drug carriers, *Ther. Deliv.* **9**, 303 (2018).
- [82] B.-W. Park, J. Zhuang, O. Yasa, and M. Sitti, Multifunctional bacteria-driven microswimmers for targeted active drug delivery, *ACS Nano* **11**, 8910 (2017).